Science & Justice xxx (xxxx) 1–12

Contents lists available at ScienceDirect

Science & Justice

journal homepage: www.elsevier.com/locate/scijus

Evaluation of photometric stereo and elastomeric sensor imaging for the non-destructive 3D analysis of questioned documents – A pilot study

Justin Gould, Simon Clement *, Bradley Crouch [1], Roberto S.P. King

Foster + Freeman Ltd, Vale Park, Evesham, Worcestershire WR11 1TD, United Kingdom

ARTICLE INFO

Keywords:
3D
Questioned documents
Photometric stereo
Elastomeric sensor imaging

ABSTRACT

Photometric Stereo and Elastomeric Sensor Imaging were assessed for measuring the 3-dimensional (3D) morphology of questioned document samples. Photometric stereo is shown to be a powerful non-contact technique for revealing micron level detail of the samples examined. Elastomeric Sensor Imaging is shown to complement photometric stereo by yielding equivalent results. Additionally, this technique allows quantification of the morphological depth information. The techniques were applied to 2 different types of questioned document sample. Firstly, written signatures were examined. Both techniques were able to reveal characteristic features that could be used to infer stroke direction and ink line application sequence. Secondly toner/ink intersections were examined. Both techniques allowed visualisation of 3D features which were used to infer the sequence of application.

1. Introduction

Questioned document examinations are commonly performed in 2 dimensions (2D). A typical examination could involve the observation of features under various illumination geometries of white light in 2 dimensions. Attempts would be made to identify and then compare features such as line quality, word and letter spacing, size consistency, pen stop, connecting strokes, letter completeness and pen pressures [1,2].

Examinations might involve analysing ink line intersections. The application sequence or the stroke direction might be inferred from observation of the migration of one ink line into another or the observation of ink of one line being dragged into another [3]. For other types of intersection, such as pen ink/laser toner, optical methods identifying spectral reflections, relative sheen, skipping and gaps in ink distribution have been utilised for the purposes of sequencing [4]. Many of these comparisons rely on the document examiners expertise and experience.

Techniques which probe the 3D morphology of questioned document features are less widely reported. LIDAR, Photogrammetry, and other 3D imaging techniques, whilst researched and applied in other areas of forensic science such as footwear analysis [5,6], odontology [7], ballistics [8] and toolmark analysis [9], are less widely reported in the analysis of questioned documents. This may be in part due to the implementation cost and/or the resolution of these techniques, with the inability to probe the 3D morphology to micron level precision.

There is some research work which is starting to explore the 3D morphology of documents. Optical coherence tomography (OCT) has been applied successfully to the analysis of both intersecting lines [10] and laminated security documents [11]. 3D laser profilometry has been used to determine the sequence of intersecting lines [12] and degree of indentation [13]. Confocal [14] and atomic force microscopy [15] have also been applied to probing the 3D morphology of documents. Focus variation microscopy has been used to yield 3D images of pen marks, and a model developed to infer which was the writing hand [16]. A recent study has used a novel 3D imaging technique to quantify pen pressure during ink line application [17]. These techniques whilst yielding useful results may require highly skilled operatives to use expensive and complex instrumentation to obtain results. Or the techniques may lack the resolution required to resolve 3D document features which are useful for a questioned document examination.

It was the aim of this study to explore the use of two different, but complementary techniques to examine the 3D morphology of questioned document samples. The two techniques investigated herein are Photometric Stereo (PS) and Elastomeric Sensor Imaging (ESI).

PS [18] is used as a non-contact method to yield semi-quantitative 3D information. This technique is straightforward and cost effective to implement and has been used widely in other scientific areas such as analysis of skin moles [19] and crop inspection [20]. Within forensic science PS has been used extensively in ballistics, for imaging of striation marks and firing pin indentations [21]. Within questioned docu-

* Corresponding author.
E-mail address: simon.clement@fosterfreeman.com (S. Clement).
[1] Present address: Eyoto Group Limited, Faraday Wharf, Holt Street, Birmingham B7 4BB, United Kingdom.

https://doi.org/10.1016/j.scijus.2023.04.016
Received 4 January 2023; Received in revised form 27 April 2023; Accepted 30 April 2023
1355-0306/

Fig. 1. (a) Illumination geometry for PS, **(b)** 4 images obtained with different angles of illumination, **(c)** results of PS algorithm to generate 3D surface map.

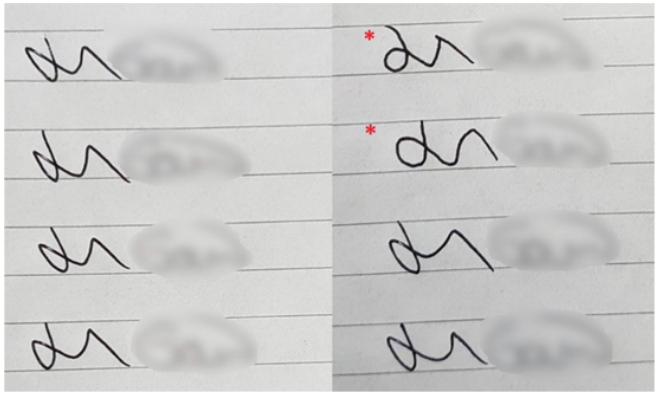

Fig. 2. Signature samples used in this study. The 2 simulated signatures are denoted with a red Asterix. The latter part of each signature has been intentionally blurred to protect the anonymity of the author. The first letter of the signature is **'j'**, whilst the second letter is **'n'**. (For interpretation of the references to colour in this figure legend, the reader is referred to the web version of this article.)

ment examination, the reported uses in the scientific literature are limited. PS has been used to resolve handwriting from background printing [22], and to form the basis of a paper classification scheme [23]. More recently it has been applied to revealing the surface topology of documents [24].

ESI [25] is implemented through the proprietary GelSight™ Mobile device which yields depth information on a smaller area of view compared to PS. This is a newer technique than PS but is being used widely in areas such as inspection of surface defects, weld inspection and hole diameter measurement. In forensic science, ESI has been used for imaging and analysis of striated and impressed tool marks for firearm identification [26] as well as imaging of post-mortem fingerprints [27]. Unlike PS it can give quantitative information about the 3D morphology being probed.

To assess the potential usefulness and limitations of both techniques, two commonly encountered Questioned Document scenarios are examined. Firstly, imaging of signatures is investigated; to reveal 3D morphological features to try to determine the ink line application sequence and stroke direction. Secondly, toner and ink intersections are examined; to try to determine the sequence of application.

2. Materials and methods

2.1. Technical background

PS is a non-contact and non-destructive technique which involves generating a map of surface normal vectors from two or more images taken with different incidence angles of illumination.

In the implementation of PS utilised in this paper, 4 images were recorded with identical camera settings with 4 different angles of illumination provided by white or IR (wavelength centred at 850 nm) LEDs. A schematic of the illumination geometry is shown in Fig. 1.

The 4 images were used to generate a surface normal map or "bumpmap" as follows. For the implementation of PS used in this work it is assumed that the sample is a Lambertian scatterer, and the incident light rays are parallel. Non-glossy paper is strongly scattering and approximates well to a Lambertian scatterer [28,29]. The LEDs are positioned approximately 202 mm horizontally and 170 mm vertically from the centre of the image, with varying azimuthal angles. The field of view used for PS is 18.3 × 13.7 mm, giving a maximum variation of the angle of incidence of the light rays across the image of 1.3 degrees. Therefore, the assumption that the incident light rays are parallel is also valid.

The intensity of each pixel is then given by.

$$\boldsymbol{I} = \boldsymbol{L}\rho\boldsymbol{n} \tag{1}$$

where **I** is the observed intensity vector, **L** the illumination matrix, ρ is the albedo and **n** the unit vector. As there are more than 3 images used in the implementation of PS in this paper, the inversion of Eq. (1) is achieved using the pseudo-inverse $(\boldsymbol{L}^T\boldsymbol{L})^{-1}\boldsymbol{L}^T$ yielding an equation for the surface normal vectors:

$$(\boldsymbol{L}^T\boldsymbol{L})^{-1}\boldsymbol{L}^T\boldsymbol{I} = \rho\boldsymbol{n} \tag{2}$$

The product of surface normal and albedo is then calculated for each pixel giving a "bumpmap". A comprehensive description of this process is given here [18]. Numerical integration of the surface normal map yields a reconstructed 3D surface or depth map. Details of this process can be found here [30].

One of the drawbacks of PS is the introduction of low frequency errors, which results in the fine detail being superimposed on a warped, rather than flat surface. To minimize this effect, the assumption is made that the samples being examined are nominally flat. The raw data from the 3D surface map calculation is fitted to a 4th order polynomial or

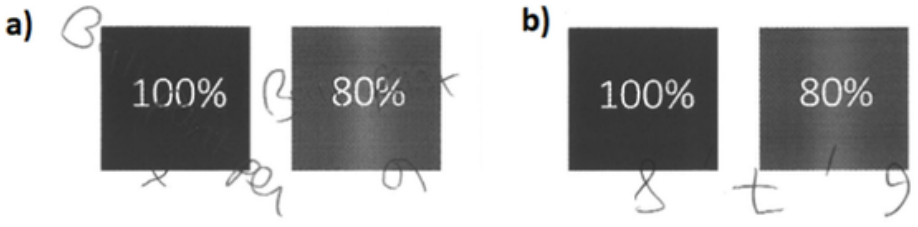

Fig. 3. Toner/ink intersection samples where **(a)** the toner was applied first, pen mark applied second, and **(b)** the pen mark was applied first, toner applied second.

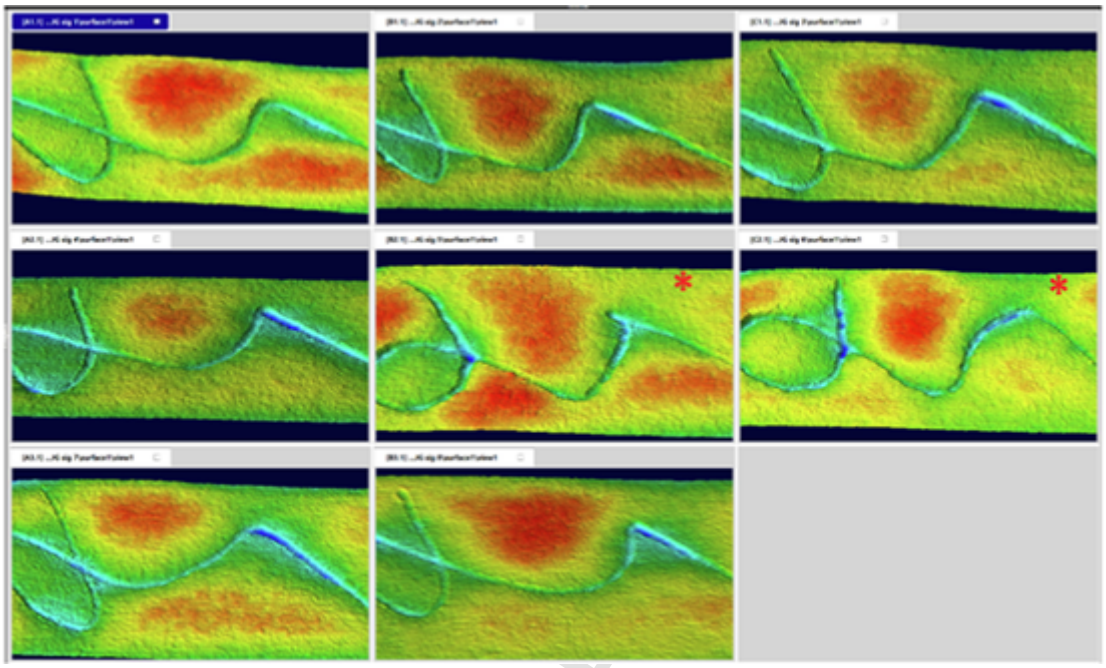

Fig. 4. "Jn" region captured using the Photometric Stereo (PS) option on the VSC8000/HS, in false colour mode and shown as a depth map. The colours range from dark blue (lowest point) to red (highest point) in the depth map. The 2 simulated signatures are denoted by a red asterisk. (For interpretation of the references to colour in this figure legend, the reader is referred to the web version of this article.)

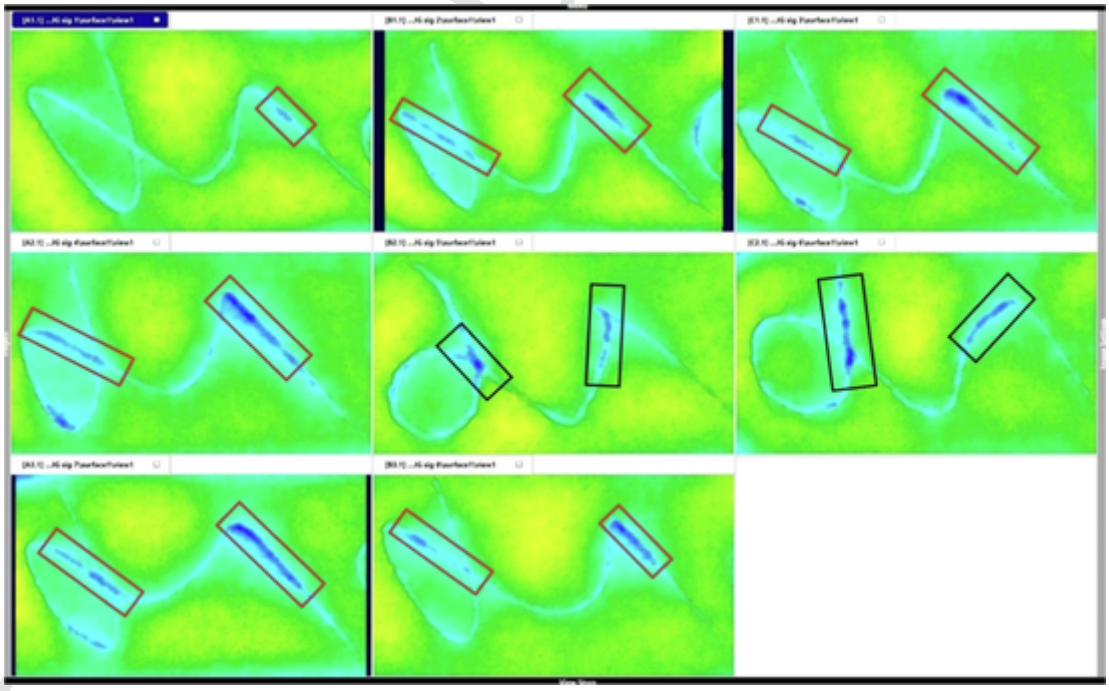

Fig. 5. PS colour map highlighting the areas of difference between the natural and simulated signatures. There were consistent differences between the natural and simulated signatures as marked below. The dark-blue areas indicate areas where greater impression is made. Red box = natural signature, Black box = simulated signature. (For interpretation of the references to colour in this figure legend, the reader is referred to the web version of this article.)

quartic surface, and this calculated surface subtracted from the raw data to yield a flattened overall 3D surface model showing the high frequency 3D features.

ESI utilises an elastomeric sensor, which is placed in contact with the sample. The deformation of the gel due to the interaction between the elastomer and the surface of the sample in question is probed using PS on rear surface of the gel to yield a 3D reconstruction of the surface [25].

2.2. Samples – Signatures*

A set of 8 signatures were prepared by one of the authors of this study, as illustrated in Fig. 2.

Six signatures were prepared in a natural manner. These are referred to as the **natural signatures** in this study. Two signatures were written in the reverse direction by the non-dominant hand, with an attempt to make the signature appear as similar as possible to the nor-

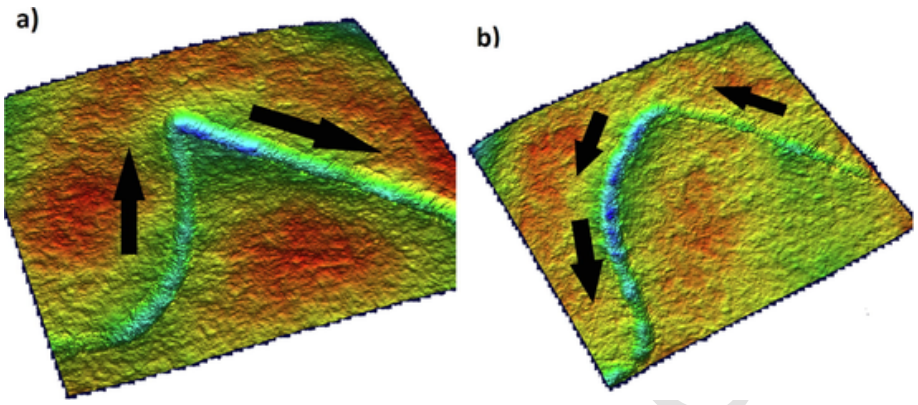

Fig. 6. relief map of natural (**a)** and simulated, (**b)** signatures highlighting the indentation depth differences on the letter **'n'**. The arrows in the figures indicate the direction of stroke.

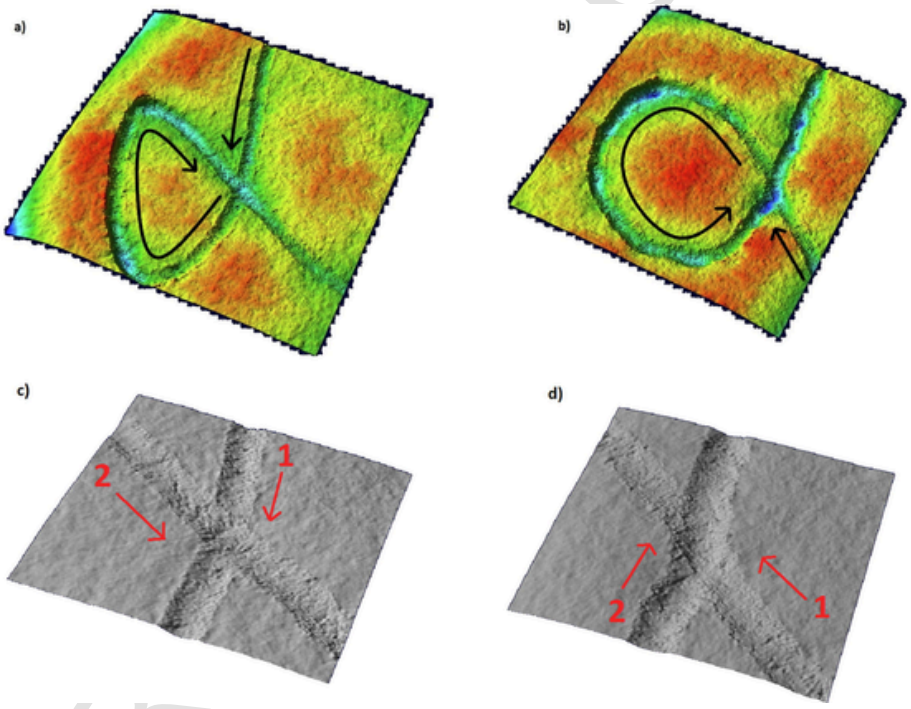

Fig. 7. relief map of natural (**a)** and simulated, (**b)** signatures highlighting the indentation depth differences on the letter 'j'. The black arrows indicate the pen direction. (**c)** and (**d)** show the intersection regions of (**a)** and (**b)** in higher magnification, respectively. The application sequence and stroke direction of and are labelled with **1** indicating the first stroke of the intersection and **2** indicating the second. The direction of application is indicated by the arrows in the figures.

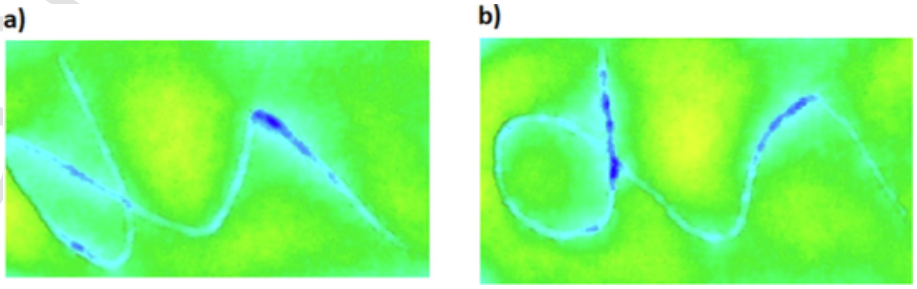

Fig. 8. Signature heatmaps obtained by PS. Image (**a)** shows the depth heatmap from the natural signature, whilst images (**b)** shows the depth heatmap from a simulated signature.

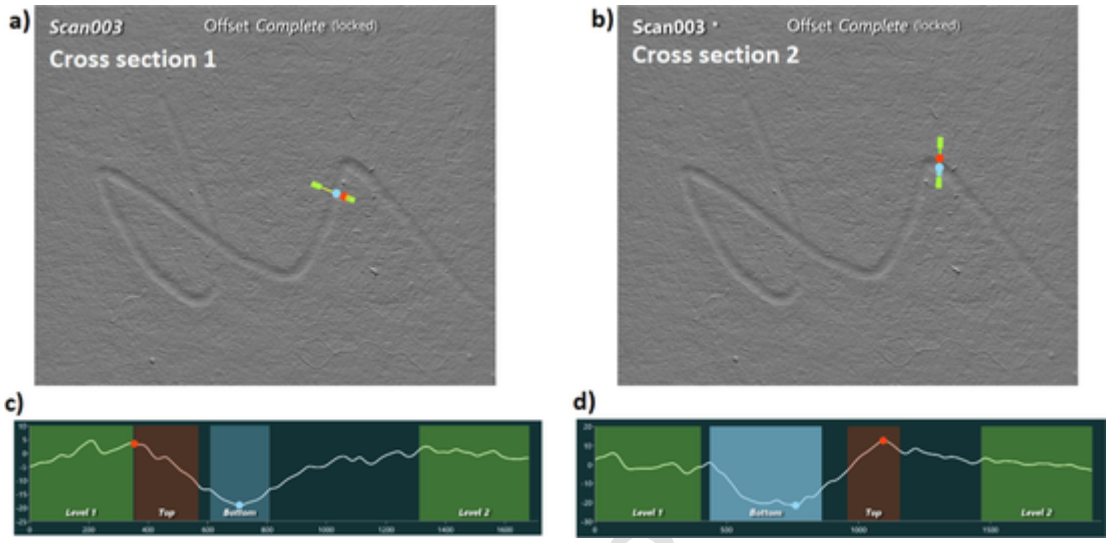

Fig. 9. depth measurements on specific areas of a simulated signature using ESI. (**a)** and (**b)** show cross-sectional regions 1 and 2 respectively in the natural signature. Whilst (**c)** and (**d)** show the corresponding measured depth graphs of cross-sectional regions 1 and 2, respectively. In both figures (**c)** and (**d)**, the x-axis measures the length of the cross-sectional area being sampled in microns, whilst the y-axis measures depth in microns.

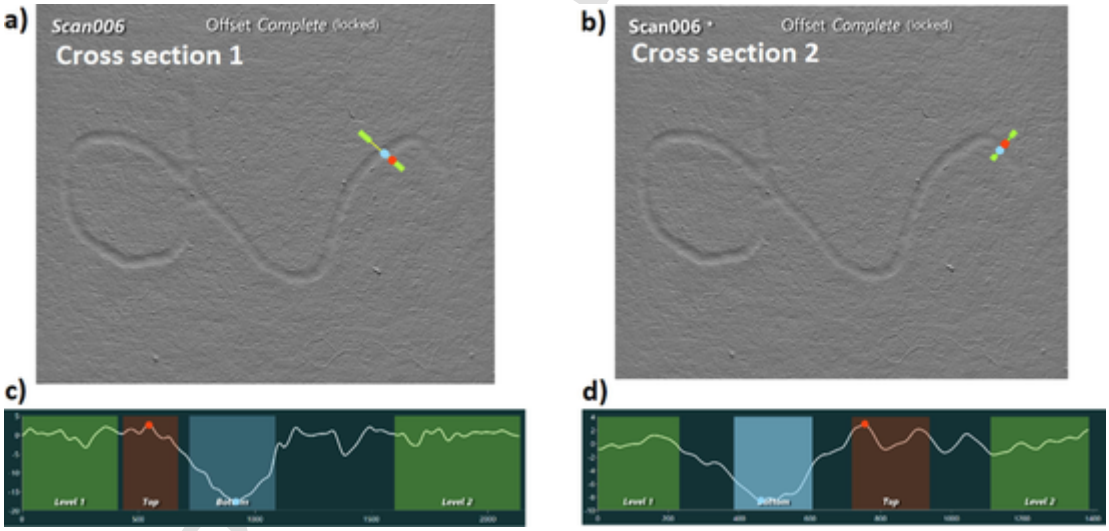

Fig. 10. depth measurements on specific areas of a simulated signature using ESI. (**a)** and (**b)** show cross-sectional regions 1 and 2 respectively in the simulated signature. Whilst (**c)** and (**d)** show the corresponding measured depth graphs of cross-sectional regions 1 and 2, respectively. In both figures (**c)** and (**d)**, the x-axis measures the length of the cross-sectional area being sampled in microns, whilst the y-axis measures depth in microns.

Table 1
Maximum cross-sectional depths obtained using the GelSight device.

Signature	Approx. depth at Cross Section 1 (microns)	Approx. depth at Cross Section 2 (microns)
Natural	22.53	34.01
Simulated	20.33	11.42

mally written signatures. These are referred to as the **simulated signatures**. The two simulated signatures were intentionally placed in amongst the natural signatures to specifically disrupt the writing flow. Other methods of signature application, for example, using a range of authors were not considered in this pilot study. The signatures were written on a single page of lined notepad paper (Initiative Shorthand Notebook), which was left on top of other papers in the pad to allow for a realistic scenario for creating indentations in the paper. The signatures were written using a black hybrid gel pen (uni-ball JETSTREAM 101) with 1 mm point size. The pen was chosen as the ink was not

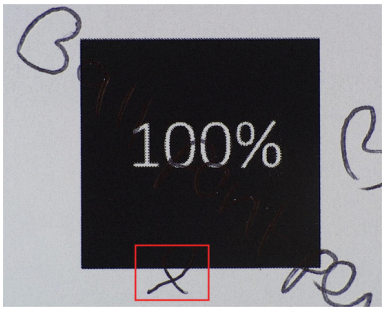

Fig. 11. The area examined in detail on both samples is highlighted in red. (For interpretation of the references to colour in this figure legend, the reader is referred to the web version of this article.)

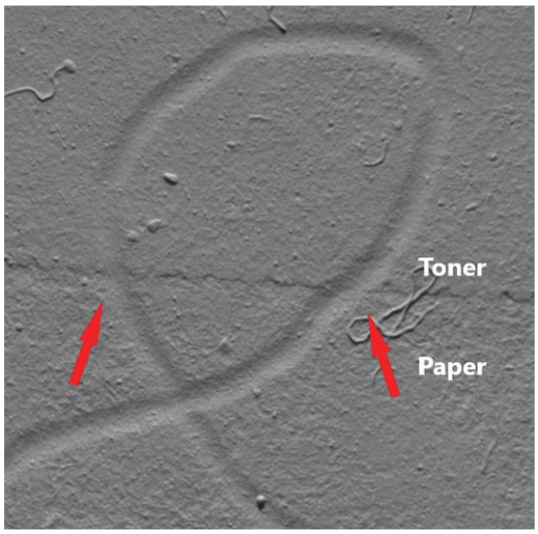

Fig. 12. The pen mark/toner intersection. toner first, pen mark after. Red arrows indicate the toner/pen mark intersection. (For interpretation of the references to colour in this figure legend, the reader is referred to the web version of this article.)

transmissive in the near-IR, thus making it harder to visualise indentation details using techniques such as near-IR oblique lighting. The authors note that the exercised force used to produce an ink line can differ between different types of writing instruments. An investigation of applying the techniques discussed in this paper to ink lines produced by other types of instruments is outside the scope of this present work.

* The aim of this pilot study was to introduce two novel techniques and highlight the advantages and pitfalls of both when applied to commonly encountered scenarios in questioned documents examination. The authors wish to highlight that the signature samples used in this work are not expected to be fully representative of those commonly encountered in genuine casework.

2.3. Samples – Ink toner intersections

Intersecting toner/ink samples were generated using a black ball point pen and a Brother HL-2030 monochrome laser jet printer. Standard A4 office paper (Nu Copier Paper A4 70 gsm) was used to produce a test print. A black ballpoint pen (Bic® Cristal ballpoint pen, with 1 mm point size) was chosen as they are commonly encountered writing implements and are known to indent the material being written on. Two samples were produced: Fig. 3a, where the test page was printed first and then pen marks applied to the document afterwards and Fig. 3b, where the pen marks were applied to the document first and then the test page printed afterwards.

The authors note that the example above is only one scenario which might present to a QD examiner - in the case of examining printed seals or graphics. Other scenarios such as the crossing of narrowly printed toner line with ink lines have not been explored in this article.

2.4. Instrumentation

The VSC®8000/HS (foster + freeman Ltd, Evesham, UK) and GelSight Mobile™ 0.5X device (GelSight, Waltham, MA, USA) were used in this study. The VSC8000/HS ff3D/Photometric Stereo software (v 2.0.14.0) option was used to generate the 3D surface maps, whilst the GelSight device was used to probe similar areas of the signatures and provide depth quantification information for the region examined.

The VSC analysis was performed in both the visible (400–700 nm) and NIR (850 nm) spectral regions for the case of the toner/ink intersection, and in the visible (400–700 nm) spectral region for the signatures. Four images were taken at differing angles of incidence of illumination which were pre-determined by the manufacturer. The surface normal and surface maps were calculated as described above. The field of view for the PS performed with the VSC was 18.3 × 13.7 mm for the work on signature and 10.7 × 8.1 mm for the work on toner/ink mark intersections. The VSC8000/HS incorporates a motorized zoom lens, and the optical zoom was set to approximately 20x to obtain this field of view. No digital zoom was applied. The images obtained were recorded at the full camera resolution of the instrument which is 12 MP.

The GelSight device was used according to the manufacturer instructions by applying the gel pad directly onto the document, so it was in direct contact with the region of interest. To ensure consistency between measurements, sufficient pressure was applied to ensure that the gel was in contact with the area shown in the camera field of view. The area probed by the GelSight device was 17.0 × 14.2 mm. The quoted X-Y spatial resolution of the GelSight device was approximately 4 μm. The quoted error bound in the Z direction was 4 μm + (4%) * Z where Z is nominal depth of the groove. The accuracy of the instrument was checked periodically during the measurements using a supplied calibration standard which was a 500 μm deep grooved target. The measured accuracy was found to be < 0.1 %.

3. Results and discussion

3.1. Signature examination

Initial examination of the 2D images of the signatures shown in Fig. 2, reveals potential differences between the natural and simulated signatures, based on the differences in circularity i.e., closeness to a circle, of the first letter **'J'** and the curvature of the top of the peak of the sec-

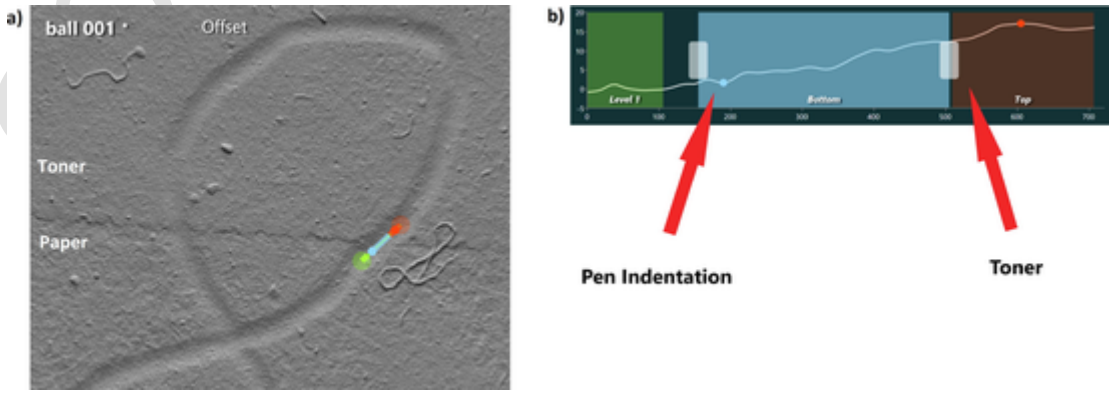

Fig. 13. (a) shows the area used to quantify the depth profile along the ink line. **(b)** shows the variation of depth along the measured area.

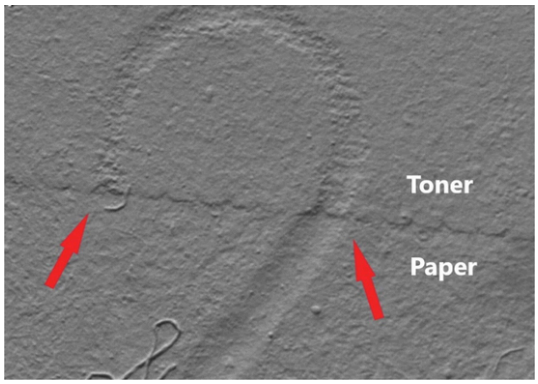

Fig. 14. Pen mark was applied first, and the toner printed second. Red arrows indicate the toner/pen mark intersection. (For interpretation of the references to colour in this figure legend, the reader is referred to the web version of this article.)

ond letter **'n'**. To further probe these potential differences, PS was applied to each signature, in turn, specifically targeting these features. Fig. 4 shows the PS images obtained as coloured surface depth map. Colours range from dark blue (lowest point) to red (highest point).

Fig. 5 shows the signatures from a direct top-down perspective and with the depth/height colours reduced for clarity (by reducing range of colours in the colourmap to blues, yellows, and greens). Differences in the morphology of the **'J'** and **'n'** in the signatures are clearly revealed. The surface of the paper is represented by green and yellow colours, the indentations from the signature are represented by the light blue and dark blue colours. The variation seen in the light blue/dark blue areas is of particular interest. The dark blue colours indicate regions of greatest depth and thus the contrast of light blue to dark blue shows differences in applied pen pressure.

All the natural signatures show a dark blue region on the righthand side of the letter **'n'** - a downwards stroke to finish that part of the signature. The two simulated signatures show a dark blue region on the opposite, left-hand side of the letter **'n,'** compared to the natural signatures. This also constituted a downward stroke since this part of the signature was produced in reverse. The PS technique shows that there is a preference for more pressure to produce the downstroke of the letter **'n'** in the signature compared to the upstroke. The observation that a downstroke has more pressure during its application compared to an upstroke has been reported previously [31]. The experiment is controlled, so the observation is consistent with the known trajectory. In this example, changing the direction of the signature (and from dominant to non-dominant hand) led to differences in where the emphasis of the stroke appears.

This is further revealed when looking at a 3D relief plot of the letter **'n'**, shown in Fig. 6.

It was also noted that the letter **'J'** also demonstrated some characteristic 3D features. The simulated signature showed emphasis of pressure on what would be the up stroke of the **'J,'** whereas with the natural signatures there was more emphasis of pressure within the loop of the **'J'**. This is revealed in Fig. 7.

It was also observed that the cross-over of the loop of the **'J'** was able to indicate the direction of the stroke and the intersection sequence. The direction of the stroke was determined at the cross-over point, providing scope for the sequencing of intersecting lines by this method. The application sequence can be determined observing the continuity or discontinuity of the ink lines which constitute the intersections. This is shown in **c)** and **d)** of Fig. 7 where the intersection region is shown in higher magnification. The ink lines are labelled "1″ and "2″ indicating the application sequence of the lines in the intersection. The stroke direction (indicated with arrows) can be inferred by noting that the cross-over loop of the **'j'** is a continuous stroke made without the pen leaving the paper. These results are consistent with other work in this area [12].

The findings from the PS examination (shown as heatmaps in Fig. 8a and 8b**)** - specifically the way that the emphasis of the pen mark pressure changed sides on the letter **'n'** were also examined by ESI. One advantage of the ESI system is the capability to quantify the depth of the indentations created when writing the signatures, thus providing quantifiable data to support the findings of the PS technique. Two regions of the letter **'n'** in the signature were identified for depth measurement using ESI technique on GelSight device. These cross-sectional regions are shown in Fig. 9 **(**natural) and Fig. 10 (simulated), along with the respective cross sectional depth graphs.

Table 1 shows the cross-sectional depth measurements of these areas for both the natural and simulated signatures. The reversal of the depth profile between the natural and simulated signature is readily observed from these measurements and is consistent with the respective 3D colour depth/height maps shown in Figs. 9 and 10. The depth measurements were made by subtracting minimum from the maximum measurement obtained from the selected cross-sectional regions. This is method used for all subsequent depth methods reported in this article.

The results of both PS and ESI examination of the sets of signatures have been shown to be able to readily yield 3D morphological features which can be used to infer both stroke direction and ink line application sequence. The advantage of ESI in this study is that it negates any potential influence from absorption/ink albedo, or assumptions about the Lambertian scattering nature of the sample. Both these effects can potentially induce errors in the calculation of the surface normal map which then propagate through to errors or artefacts in the reconstruction of the 3D surface map. Additionally, quantification of the depth

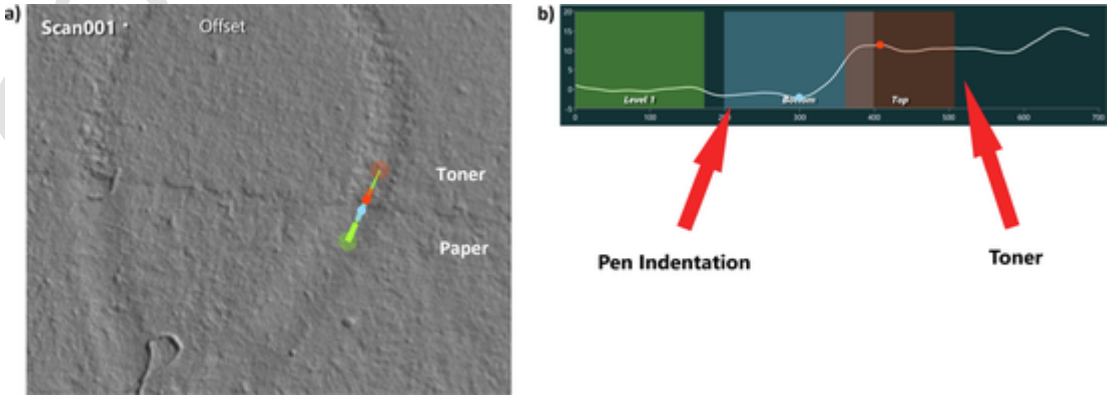

Fig. 15. (a) shows the area used to quantify the depth profile along the ink line. **(b)** shows the variation of depth along the measured area.

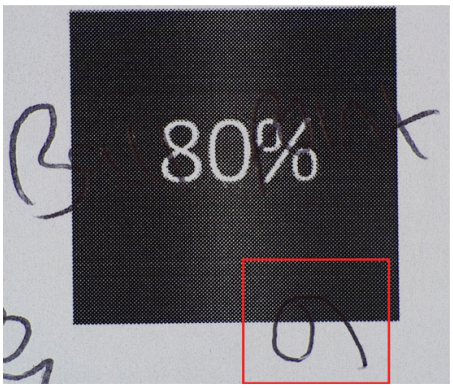

Fig. 16. Toner first /pen mark second. 80% toner. region examined highlighted in red. (For interpretation of the references to colour in this figure legend, the reader is referred to the web version of this article.)

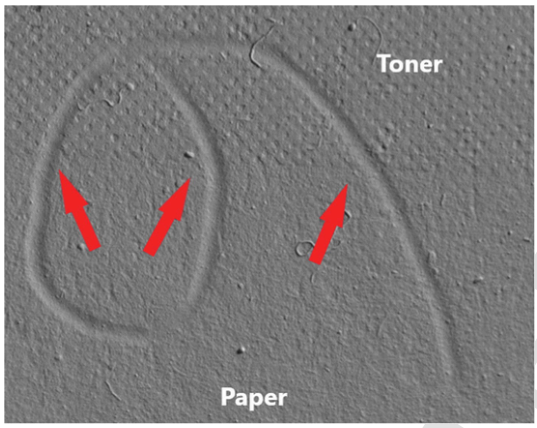

Fig. 17. Toner first/pen mark second. '80% toner feature'. textured detail diminished/obliterated. Red arrows indicate the toner/pen mark intersection. (For interpretation of the references to colour in this figure legend, the reader is referred to the web version of this article.)

gives the ESI technique scientific robustness over PS, which is arguably a subjective analysis that must be conducted by an experienced examiner.

However, it is prudent to note that whilst PS is a non-destructive and non-contact technique, ESI requires direct contact and pressure, albeit minimal, to be applied to the samples being examined. It was noted that during examination using ESI, there was, on occasion ink material transferred to the gel probe. This was more pronounced on freshly prepared ink samples. This observation might well preclude ESI from widespread use in QD examination, due to the risk of cross-contamination between samples as well as perceived surface/sample degradation. Moreover, at this stage, it is also not clear what the effect of repeated measurements using ESI on the same sample would have on the integrity of the 3D morphology. Factors which influence ink transfer to the gel probe were not explored further in this article. PS being a completely non-contact technique does not suffer from these deficiencies. It is also noted that there is potential to further enhance the accuracy of the ESI measurements, by taking the average of multiple cross-sectional regions, estimating the "ground-truth" depth of the grove created by the pen, by averaging the measurement within the groove versus the average measurement across the paper etc. This aspect of groove depth quantification is not explored further in this article.

3.2. 3D imaging of pen mark/laser printer toner intersections - ESI results

Fig. 11 shows the ink/toner intersection that was chosen for more detailed examination. The same intersection was examined on both prepared samples – toner first/ink second, and vice versa.

The examinations were conducted initially using the ESI, before applying PS to the examination of the same intersecting features.

The toner samples produced a layer of toner that could be distinguished from the substrate, in the form of a ridge. This is shown in Fig. 12**,** with the intersection points highlighted with red arrows, and the observation that the toner is 'flattened' when the toner is applied first, pen mark second.

ESI was able to provide a cross-sectional measurement of the pen mark/laser toner intersection. The area measured is shown in Fig. 13a, whilst the measurement profile is shown in Fig. 13b. It is observed that the transition across the ink line is relatively smooth, consistent with the observation that the toner is flattened by the application of the ink line.

ESI was also applied to the ink first/toner second sample shown in Fig. 14. The intersection points are highlighted with red arrows. In this case it is observed that there is a continuation of the toner ridge as it crosses the ink line. This is opposite to what was observed when the toner was applied first/pen mark second.

The cross-sectional depth profile was also measured on this sample as shown in Fig. 15. There is a sharp increase in height caused by the intact toner ridge compared to the smoother cross section seen on the other sample, where the toner ridge had been flattened by the pen mark.

The same set of experiments were applied to the toner region which is marked "80%". This toner feature was specifically printed to have a lower coverage on the paper than the "100 %" feature, to investigate whether toner surface coverage might affect the results. The area examined by ESI is shown in Fig. 16 - highlighted with a red box.

The ESI results are shown in Fig. 17. It is noted in this case that the more textured nature of the toner deposition is visible in the image. As in the previous sample, the toner ridge was observed to have been flattened by the pen mark as it was drawn over the toner. Additionally, the textured pattern has been obliterated by the pen mark due to the mark being made after the toner was deposited, thus providing additional evidence that the toner was printed first.

Examining the cross-section - Fig. 18 showed the intersection to be relatively flat, where the toner ridge has been flattened by the pen mark.

However, when the pen mark was produced first and the toner printed on top, the toner ridge can be clearly observed - Fig. 19. In this instance we can also see that the toner texture is still present due to it being printed after the pen stroke had been made. The effects of this textured pattern can be observed in the cross section - Fig. 20**.** The toner ridge and the textured pattern, giving a roughened effect compared to the smoother cross-section observed where the pen mark obliterated the textured toner pattern.

3.3. 3D imaging of pen mark/laser printer toner intersections - Photometric Stereo results

The same samples were then analyzed using PS. The initial experiments were conducted with visible light illumination and then repeated using NIR LED illumination centered at 850 nm. The rationale for this is that the ink used becomes transmissive in the NIR so any effects from the ink absorption/albedo should be minimized.

Fig. 21 shows the results of PS performed in the visible part of the spectrum on a 100% toner printed sample. There are indications that the toner ridge is still present across the ink line when the pen mark was applied first. This was absent when the pen mark was applied second.

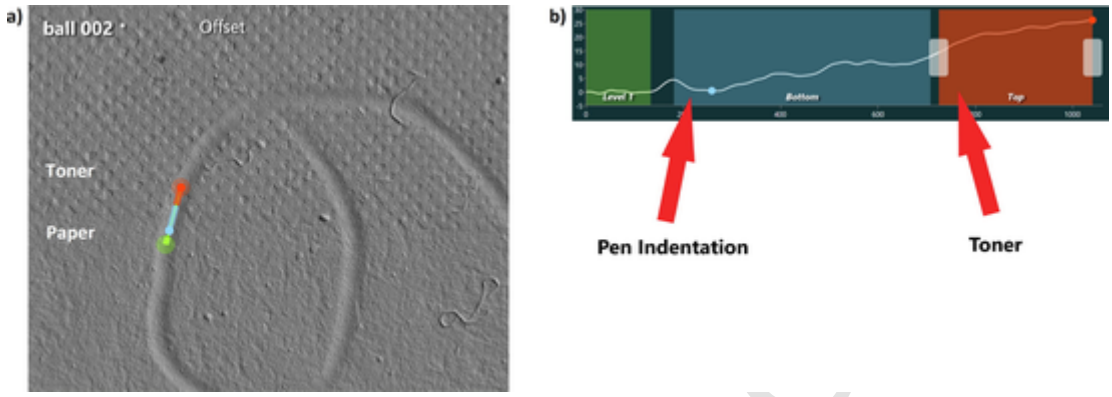

Fig. 18. (a) shows the area used to quantify the depth profile along the ink line. (**b)** shows the variation of depth along the measured area.

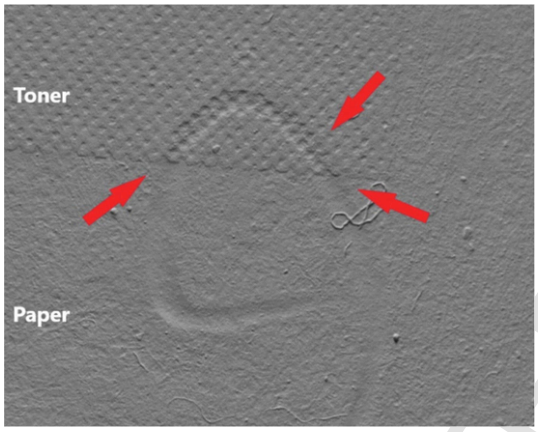

Fig. 19. ink mark was produced first, and the toner printed on top. Red arrows indicate the toner/pen mark intersection. (For interpretation of the references to colour in this figure legend, the reader is referred to the web version of this article.)

PS using NIR (850 nm) was also performed on the same sample. The results are shown in Fig. 22 but did not yield any different information when compared to the same experiments performed in the visible spectral region.

The "80%" samples (i.e., with partial toner coverage of the paper) were then analyzed using the same method. The results for these samples analyzed in visible and NIR (850 nm) illumination are shown in Figs. 23 and 24**,** respectively. The textured pattern from the toner can be readily observed, with the toner pattern being more prominent when the pen mark is applied first. Both these results are consistent with the results obtained using ESI. However, when using the NIR (850 nm) illumination (as illustrated in Fig. 24**),** the observation of the indentation from the pen when the pen mark is applied prior to the toner, seems to dramatically diminish.

When the toner coverage of the samples was complete (100 % sample), ESI gave superior results to PS for inferring the sequence of application of the on the toner/pen mark. This was the case irrespective of whether PS had been performed in the visible or NIR (850 nm) spectral region – where the ink becomes transparent. This may be due to the toner absorbing through the visible and the NIR (850 nm), which means that even though the ink becomes transmissive in the NIR (850 nm), the toner underneath the pen stroke will still absorb. Although it is noted that PS gave results that might lead an experienced QD examiner to infer the sequence of the application, the results were less conclusive than the ESI results.

For the case when the toner only partially covered the paper (the 80% sample), ESI and PS gave complementary results when PS was performed in the visible spectral region. When PS was performed in the IR on the same samples, the 3D grove produced by the pen mark Fig. 24 **Pen 1st**, was no longer readily observed. The cause of this observation was not immediately clear. However, the authors note that the VSC8000/HS is designed to maximize optical resolution and quality in the visible spectral region, so it might be that the increased optical aberrations in the NIR, may degrade the effectiveness of PS performed at 850 nm.

4. Conclusions

PS and ESI examination of documents have shown to be powerful tools in revealing and quantifying depth profiles in handwritten documents. When applied to signature analysis, they produced similar and

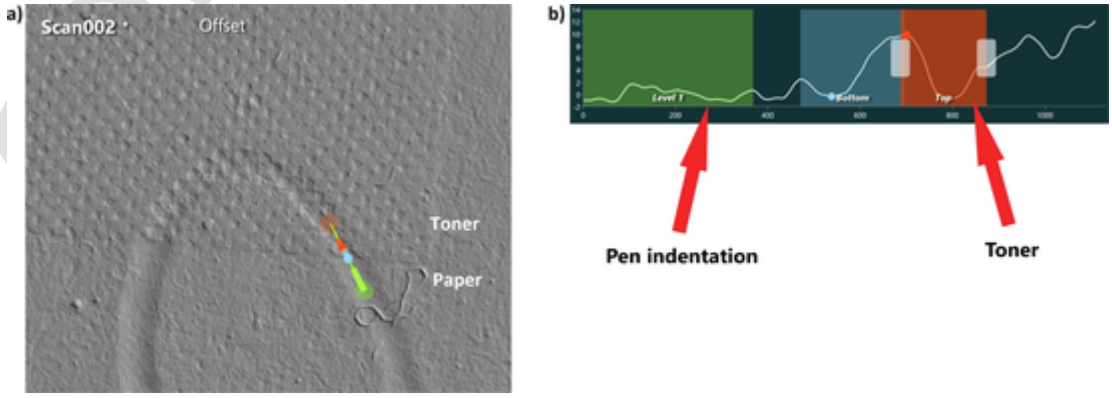

Fig. 20. These effects can be observed (and measured) in cross section showing both the toner ridge and textured pattern. **(a)** Shows the area used to quantify the depth profile along the ink line. **(b)** Shows the variation of depth along the measured area.

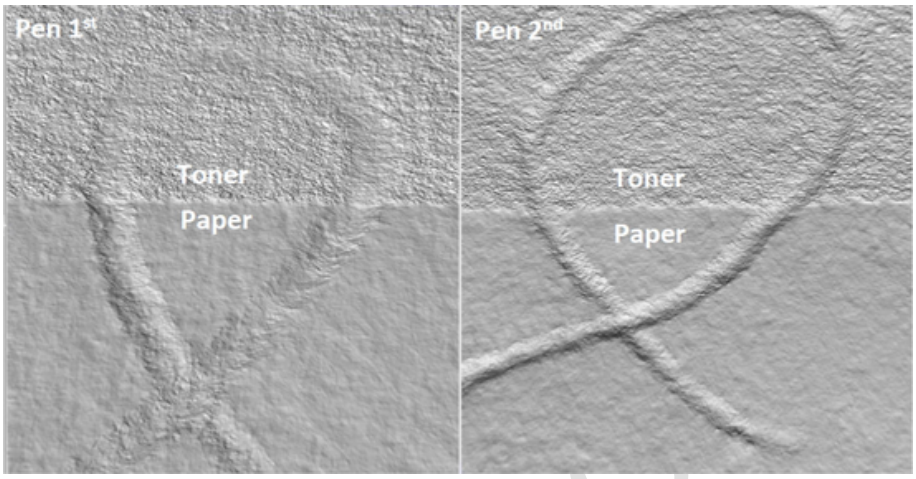

Fig. 21. PS performed in the visible. Indications of the toner ridge can be observed where the pen mark was made first.

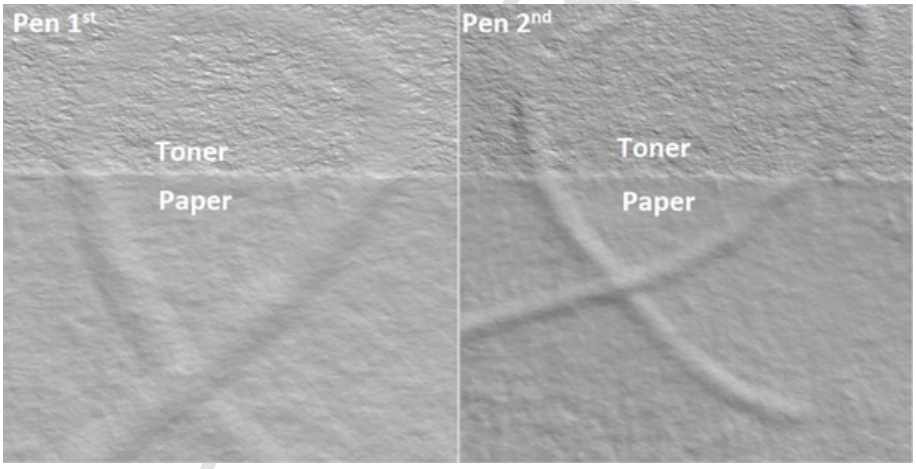

Fig. 22. PS performed in the near-IR.

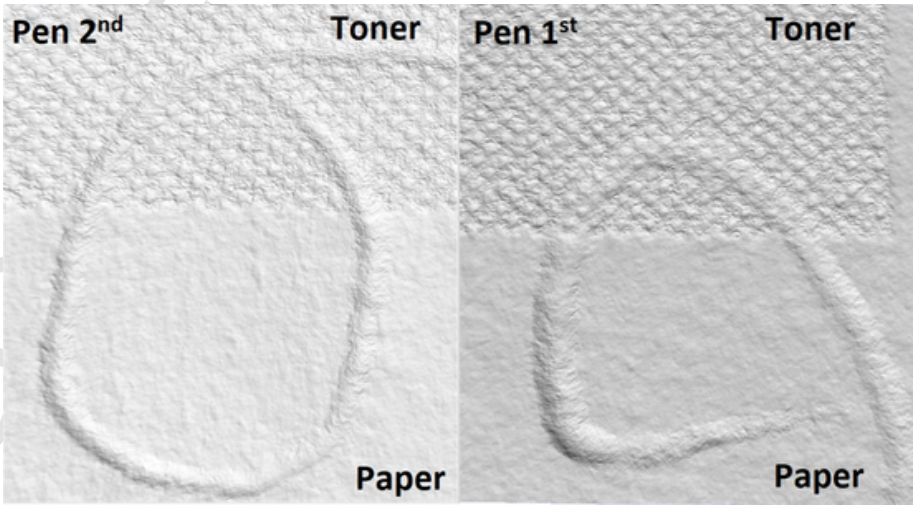

Fig. 23. 80% toner. PS performed in the visible.

complementary results. Both techniques were able to reveal characteristic 3D features to aid the questioned documents examiner. The quantification afforded by the ESI method added additional scientific robustness to the conclusions. When applied to toner/ink intersection sequence determination both techniques allowed inference of the application sequence of the toner/ink. ESI was superior to PS when there was heavy coverage by the toner component. The results were equivalent when there was only partial coverage by the toner.

The advantages and drawbacks of each technique were discussed. In the case of ESI, the fact that the probe had to be in direct contact with

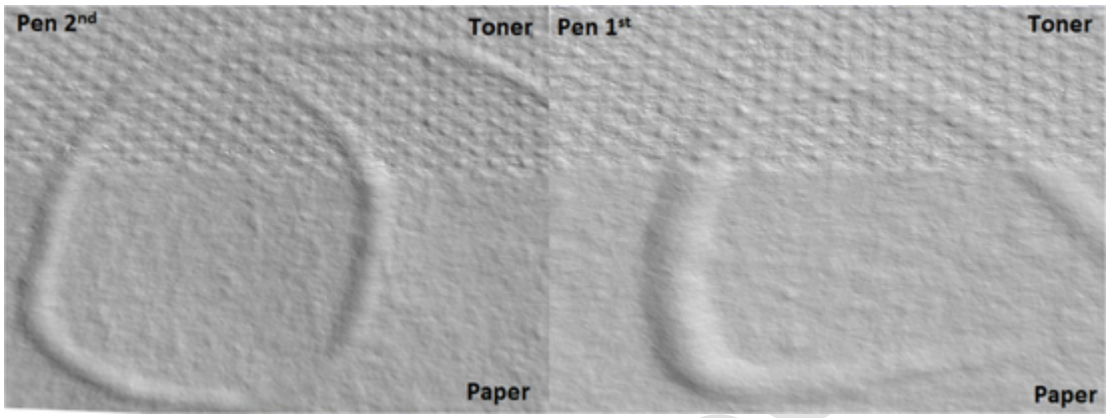

Fig. 24. 80% toner. PS performed in the IR (850 nm LED).

the sample was deemed to be a disadvantage compared to PS which is non-contact. Whilst PS can be prone to artefacts/errors due to the absorption/albedo of the ink, which was not a problem with ESI.

4.1. Future work

Future work will focus on three areas:

- The inference of stroke direction of the crossing intersections. The potential for this was observed during signature examination using PS. This observation has not been explored further in this paper and will form the basis of future work.
- Quantification of the results of PS. The current implementation of PS in the VSC8000/HS is semi-quantitative, whilst ESI gives a quantitative depth measurement. Future work will attempt to fully quantify the PS implementation in the VSC8000/HS, and therefore increase the scientific robustness of the results.

Declaration of Competing Interest

The authors declare that they have no known competing financial interests or personal relationships that could have appeared to influence the work reported in this paper.

Acknowledgements

Many thanks to Gelsight/Sempre group for loan of a Gelsight system. Thanks also to Darren Corbett and Peter Hallett (foster + freeman) for assistance with the graphics, and clarification of the optical engineering aspects of the VSC8000/HS.

References

[1] H.C. Rile, Identification of signatures, in: J.S. Kelly, B.S. Lindblom (Eds.), Scientific Examination of Questioned Documents, CRC Press, New York, 2006, pp. 75–108. https://doi.org/10.1201/9781420003765.
[2] European Network of Forensic Science Institutes (ENFSI), Best Practice Manual for the Forensic Evaluation of Handwriting (ENFSI-BPM-FHX-01), Issue 04 - September 2022. https://enfsi.eu/wp-content/uploads/2022/12/4.-BPM-Edition-4-Draft-20220822-3-1.pdf.
[3] Interpol, Physical-Chemical study of Crossed Line Intersection, https://www.interpol.int/en/Crimes/Counterfeit-currency-and-security-documents/Physical-Chemical-Study-of-Crossed-Line-Intersection#:~:text=We%20are%20developing%20a%20new,document%20was%20forged%20or%20falsified.
[4] K. Saini, R. Kaur, N.C. Sood, Determining the sequence of intersecting gel pen and laser printed strokes — a comparative study, Sci. Justice 49 (2009) 286–291, https://doi.org/10.1016/j.scijus.2009.07.003.
[5] T.J.U. Thompson, P. Norris, A new method for the recovery and evidential comparison of footwear impressions using 3D structured light scanning, Sci. Justice 58 (2018) 237–243, https://doi.org/10.1016/j.scijus.2018.02.001.
[6] H. Larsen, M. Budka, M.R. Bennett, Technological innovation in the recovery and analysis of 3D forensic footwear evidence: structure from motion (SfM) photogrammetry, Sci. Justice 61 (2021) 356–368, https://doi.org/10.1016/j.scijus.2021.04.003.
[7] A.B. Márquez-Ruiz, M.C. Treviño-Tijerina, L. González-Herrera, B. Sánchez, A.R. González-Ramírez, A. Valenzuela, Three-dimensional analysis of third molar development to estimate age of majority, Sci. Justice 57 (2017) 376–383, https://doi.org/10.1016/j.scijus.2017.04.002.
[8] G. Gerules, S.K. Bhatia, D.E. Jackson, A survey of image processing techniques and statistics for ballistic specimens in forensic science, Sci. Justice 53 (2013) 236–250, https://doi.org/10.1016/j.scijus.2012.07.002.
[9] X.A. Zheng, J. Soons, R. Thompson, J. Villanova, T. Kakal, 2D and 3D topography comparison of toolmarks produced from consecutively manufactured chisels and punches, AFTE J 46 (2014) 143–147. https://tsapps.nist.gov/publication/get_pdf.cfm?pub_id=914887.
[10] N. Zhang, P. Jiang, W. Wang, C. Wang, L. Xie, Z. Li, W. Huang, G. Shi, L. Wang, Y. Yan, S. Gao, Initial study for the determination of the sequence of intersecting lines between gel pens, and seals by optical coherence tomography, J. Forens. Sci. 65 (2020) 2071–2079, https://doi.org/10.1111/1556-4029.14514.
[11] M.J. Marques, R. Green, R. King, S. Clement, P. Hallett, A. Podoleanu, Sub-surface characterisation of latest-generation identification documents using optical coherence tomography, Sci. Just. 61 (2021) 119–129, https://doi.org/10.1016/j.scijus.2020.12.001.
[12] G.S. Spagnolo, Potentiality of 3D laser profilometry to determine the sequence of homogenous crossing lines on questioned documents, Forensic Sci. Int. 164 (2006) 102–109, https://doi.org/10.1016/j.forsciint.2005.12.004.
[13] F. Dellavalle, S. Frontini, A preliminary study of 3D depth measurement of the grooves generated by three different pens for handwriting, J. Am. Soc. Question. Doc. Exam. 20 (2017) 37–53. https://scholar.google.com/scholar_lookup?journal=J.%C2%A0Am.+Soc.+Questioned.+Document+Exam.&title=A%C2%A0preliminary+study+of+3D+depth+measurement+of+the+grooves+generated+by+three+different+pens+for+handwriting&author=F.+Dellavalle&author=S.+Frontini&volume=20&issue=2&publication_year=2017&.
[14] M. Mann, S.R. Pathak, S.K. Shukla, Three-dimensional detection of sequence of strokes using confocal microscope, Egypt. J. Forens. Sci. 9 (2019), https://doi.org/10.1186/s41935-019-0120-z.
[15] T.Y. Kang, J. Lee, B.W. Park, Use of atomic force microscopy in the forensic application of chronological order of toners and stamping inks in questioned documents, Forensic Sci. Int. 261 (2016) 26–32, https://doi.org/10.1016/j.forsciint.2016.01.033.
[16] Y.X. Guo, B. Li, Pilot study on associating pen pressure with pen holding position using three-dimension property of stroke indentation, J. Forensic Sci. Med. 7 (2021) 152–158. https://journals.lww.com/jfsm/Fulltext/2021/07040/Pilot_Study_on_Associating_Pen_Pressure_with_Pen.6.aspx.
[17] F. Asicioglu, A.S. Yilmaz J.de Kinder, I. Pekacar, A. Gelir., A novel 3D scan-based optical method for analyzing lines drawn at different pen pressure, Forensic Sci. Int. 1 (338) (2022) 111388, https://doi.org/10.1016/j.forsciint.2022.111388.
[18] K. Ikeuchi, Y. Matsushite, R. Sagawa, H. Kawasaki, Y. Mukaigawa, R. Furukawa, D. Miyazaki, Photometric Stereo, in: S. Singh, S.B. Kang (Eds.), Active Lighting and Its Application for Computer Vision, Springer, Switzerland, 2020, pp. 107–123. https://doi.org/10.1007/978-3-030-56577-0.
[19] J. Sun, M. Smith, L. Smith, L. Coutts, R. Dabis, C. Harland, J. Bamber, Reflectance of human skin using colour photometric stereo: With particular application to pigmented lesion analysis, Skin Res. Technol. 14 (2008) 173–179, https://doi.org/10.1111/j.1600-0846.2007.00274.x.
[20] L.N. Smith, W. Zhang, M.F. Hansen, I.J. Hales, M.L. Smith, Innovative 3D and 2D machine vision methods for analysis of plants and crops in the field, Comput. Ind. 97 (2018) 122–131, https://doi.org/10.1016/j.compind.2018.02.002.
[21] U. Sakarya, U.M. Leloğlu, E. Tunalı, Three-dimensional surface reconstruction for cartridge cases using photometric stereo, Forensic Sci. Int. 175 (2–3) (2008 Mar 5) 209–217, https://doi.org/10.1016/j.forsciint.2007.07.003.
[22] G. McGunnigle, M.J. Chantler, Resolving handwriting from background printing using photometric stereo, Pattern Recogn. 36 (8) (2003) 1869–1879, https://doi.org/10.1016/S0031-3203(03)00012-8.
[23] H. Malekmohamadi, K. Emrith, S. Pollard, G. Adams, M. Smith, S. Simske, Paper

substrate classification based on 3D surface micro-geometry, in: 2014 International Conference on Computer Vision Theory and Applications (VISAPP) 2014 Jan 5, vol. 2, IEEE, pp. 448-453.
[24] İ. Baz, C. Kılıç, 3D modeling of a document surface topography with a photometric stereo method (2020) 1–4, https://doi.org/10.1109/SIU49456.2020.9302040.
[25] M.K. Johnson, F. Cole, A. Raj, E.H. Adelson, Microgeometry capture using an elastomeric sensor, ACM Trans. Graph. 30 (2011) 1–8, https://doi.org/10.1145/2010324.1964941.
[26] R. Lilien, Applied research and development of a three-dimensional topography system for imaging and analysis of striated and impressed tool marks for firearm identification using GelSight, in: Forensic Science Seminar ISSN 2015 Jan 1.
[27] M.N. Carlson, Evaluation of the GelSight Mobile™ 3-D imaging system for collection of postmortem fingerprints (Doctoral dissertation, Boston University). https://hdl.handle.net/2144/45535.
[28] F. Azhar, K. Emrith, S. Pollard, M. Smith, G. Adams, S. Simske, Testing the validity of lamberts law for micro-scale photometric stereo applied to paper substrates, 10th International Conference on Computer Vision Theory and Applications -Volume 1: VISAPP, Berlin, Germany, 2015, pp. 246–253.
[29] Y. Akao, N. Tsumura, T. Norimichi, Y. Miyake, Characterization of white paper sheets by BRDF model parameters estimated in the specular reflection plane, J. Imaging Sci. Technol. 54 (2010), https://doi.org/10.2352/J.ImagingSci.Technol.2010.54.6.060503.
[30] C. S. Verma, M.-J. Wu, Photometric Stereo. Accessed: Mar. 7, 2022. [Online]. https://pages.cs.wisc.edu/~csverma/CS766_09/Stereo/stereo.html.
[31] R.N. Morris, Ratios – Relative relationships, in: Forensic Handwriting Identification: Fundamental Concepts and Principles, Academic Press, 2020, pp 107–128.